Research Square

Preprints are preliminary reports that have not undergone peer review.
They should not be considered conclusive, used to inform clinical practice,
or referenced by the media as validated information.

Spatio-Temporal Modeling of Dengue in Argentina (2009–2025): Risk Factors, spatial patterns, and implications for prevention planning

J. Piette

josephine.piette@unamur.be

University of Namur

C. Linard

Institute of Life, Earth and Environment

C. Morlighem

NEMESIS, Institut Pierre Louis d'Epidémiologie et de Santé Publique, IPLESP, Sorbonne Université, INSERM F75012

V. Andreo

Instituto de Altos Estudios Espaciales "Mario Gulich"

Research Article

Keywords: Dengue, spatio-temporal modeling, INLA, Bayesian inference, ENSO, El Niño, Argentina, climate, Aedes aegypti, disease mapping, risk stratification

Posted Date: August 11th, 2026

DOI: https://doi.org/10.21203/rs.3.rs-10165514/v1

License: This work is licensed under a Creative Commons Attribution 4.0 International License.
Read Full License

Additional Declarations: No competing interests reported.

Spatio-Temporal Modeling of Dengue in Argentina (2009–2025): Risk Factors, spatial patterns, and implications for prevention planning

J. Piette[1,2,4], C. Linard[1,2,3], C. Morlighem[5], V. Andreo[6,7]

[1]*University of Namur, Department of Geography, 5000 Namur, Belgium*

[2] *Institute of Life, Earth and Environment (ILEE), University of Namur, 5000 Namur, Belgium*

[3] *Namur Research Institute for Life Sciences (NARILIS), University of Namur, 5000 Namur, Belgium*

[4]*Transitions Research Institute (TRANSITIONS), University of Namur, 5000 Namur, Belgium*

[5]*NEMESIS, Institut Pierre Louis d'Epidémiologie et de Santé Publique, IPLESP, Sorbonne Université, INSERM F75012, Paris, France*

[6]*Gulich Institute. Argentinian Space Agency (CONAE) and National University of Córdoba, Córdoba, Argentina*

[7]*National Scientific and Technical Research Council (CONICET), Buenos Aires, Argentina*

Corresponding author: J. Piette, University of Namur, Department of Geography, Institute of Life, Earth and Environment (ILEE), 5000 Namur, Belgium. Email: josephine.piette@unamur.be.

Abstract

Background: Dengue has expanded markedly in Argentina, with *Aedes aegypti* now established in temperate provinces and successive epidemics culminating in a record outbreak in 2024. Disentangling large-scale inter-annual climate variability from local environmental and socio-infrastructural conditions is essential for targeted prevention, yet few studies have modelled dengue determinants across Argentina's heterogeneous transmission zones at national scale. **Methods:** We analysed 817,699 dengue cases reported across 473 departments in northern and central Argentina from 2009 to 2025 using Bayesian hierarchical spatio-temporal models within the integrated nested Laplace approximation (INLA) framework. A zero-inflated negative binomial distribution accounted for overdispersion and excess zeros; spatial, temporal and space–time random effects were combined with climatic, environmental and sociodemographic covariates, and predictive performance was assessed through forward-chaining temporal cross-validation. **Results:** Dengue incidence showed strong inter-annual variability, peaking in 2024. El Niño years carried markedly higher risk independent of seasonal climate. Higher current-summer temperature and relative humidity were

associated with increased risk, while previous-spring temperature showed a non-linear carry-over relationship with subsequent transmission. Populations living near waste-disposal sites were at greater risk. The model reliably identified high-risk department-years, including the 2024 epidemic, although forecasting outbreak magnitude remained more challenging. **Conclusions:** Large-scale climate variability, seasonal weather and local environmental factors jointly shape dengue transmission in Argentina. Bayesian risk mapping can guide targeted prevention and seasonal early-warning systems, particularly along the expanding southern transmission frontier.

Keywords: Dengue; spatio-temporal modeling; INLA; Bayesian inference; ENSO; El Niño; Argentina; climate; Aedes aegypti; disease mapping; risk stratification

1. Background

Dengue fever is the most rapidly spreading mosquito-borne viral disease worldwide, with an estimated 100 million symptomatic cases and around 300 million asymptomatic infections occurring annually, placing nearly half of the global population at risk of infection [1]. Transmitted primarily by *Aedes aegypti* mosquitoes, dengue has dramatically expanded its geographic range over recent decades, driven by urbanization, globalization, and climate change [2, 3]. The 2023–2024 period witnessed an unprecedented global surge, with the Americas recording more than 4.8 million suspected cases during the first quarter of 2024 alone and Brazil reporting over 6 million cases for the season [4, 5].

In the Americas, dengue incidence has increased dramatically since the 1980s following the relaxation of *Aedes* eradication programs, with recurrent epidemics affecting millions across Latin America and the Caribbean [6]. Argentina, historically at the southern margin of transmission, has experienced a marked intensification of dengue activity in recent years. Dengue-competent *Ae. aegypti* populations have progressively expanded southward, now established in temperate central regions including Buenos Aires province [7, 8]. Entomological surveys have documented *Ae. aegypti* presence at unprecedented latitudes, including new coldest and southernmost records for South America [9, 10, 11]. This geographic expansion,

combined with increased human mobility and viral introduction events, has produced increasingly severe epidemics: the 2016 outbreak affected over 76,000 confirmed cases nationwide, while the 2020 and 2023 seasons exceeded 58,000 and 118,000 cases respectively. The 2024 season then surpassed 500,000 cases nationally — approximately a four-fold increase over the previous record — establishing year-round transmission potential in northeastern provinces [12]. A growing body of Argentine research has documented these climate–vector dynamics across temperate and subtropical sites [13, 14, 15, 16].

Climate change is accelerating the expansion of *Ae. aegypti* habitat suitability. Global analyses project that the world is becoming approximately 1.5% more suitable per decade for *Ae. aegypti* development, with this trend expected to accelerate toward 2050 [17, 18]. In South America, invasion fronts are projected to advance poleward, with temperate regions experiencing the largest proportional gains in transmission suitability. These projections underscore the urgent need for spatially explicit risk assessment tools to guide prevention planning.

Understanding the spatial and temporal drivers of dengue transmission is essential for developing targeted prevention strategies. Prior research has established the importance of climatic factors — particularly temperature, humidity, and precipitation — in modulating *Ae. aegypti* population dynamics and viral transmission efficiency [19, 20]. Temperature influences mosquito development, survival, biting frequency, and the extrinsic incubation period of the virus, with optimal transmission occurring between 21.3 °C and 34.0 °C [3]. Atmospheric humidity independently affects adult vector survival and biting behavior [21], while precipitation governs the availability of larval breeding habitats.

Beyond mean seasonal climate, inter-annual climate variability driven by the El Niño–Southern Oscillation (ENSO) has been increasingly recognized as a determinant of dengue epidemics across the Americas [22, 23, 24]. In subtropical South America, El Niño phases are associated with above-normal precipitation and warmer conditions, while La Niña phases produce drier and cooler conditions [25, 26, 27]. Because ENSO operates at seasonal-to-multiannual scales distinct from mean seasonal conditions and is forecastable several months in advance, explicitly quantifying its contribution is of direct relevance to early warning.

Socioeconomic and infrastructural factors further shape dengue risk through their influence on human–vector contact. *Ae. Aegypti* is highly adapted to urban environments, breeding preferentially in artificial containers associated with human habitation [28]. Waste accumulation provides abundant breeding habitats [29], and domestic water-management practices — including stored-water reservoirs maintained where piped supply is unreliable — are well-documented sources of vector productivity [30, 31]. Finally, reported incidence reflects not only true disease burden but also surveillance performance: passive case detection captures only an estimated 10–50% of symptomatic infections [32, 33], and ascertainment varies with healthcare access and diagnostic capacity.

Yet, despite this growing body of knowledge, no study has comprehensively characterized the spatio-temporal dynamics of dengue transmission across Argentina's heterogeneous ecological and socioeconomic landscape, nor disentangled the joint contributions of seasonal climate, inter-annual ENSO variability, and local infrastructural conditions — a gap that has become particularly acute given the unprecedented epidemic trajectory observed since 2020 and the accelerating southward expansion of *Ae. aegypti* documented through 2024**.** The objectives of this study are to: (1) characterize the spatio-temporal distribution of dengue incidence across departments in northern and central Argentina from 2009 to 2025; (2) identify climatic, environmental, and sociodemographic determinants of transmission risk, explicitly disentangling ENSO from seasonal climate effects; (3) evaluate the role of waste management and water infrastructure as risk factors; and (4) assess model performance for spatial risk stratification to support prevention planning. We employ Bayesian hierarchical modeling within the Integrated Nested Laplace Approximation (INLA) framework, which is well-suited to this setting given the strong spatial and temporal dependence in dengue incidence and the high prevalence of zero counts.

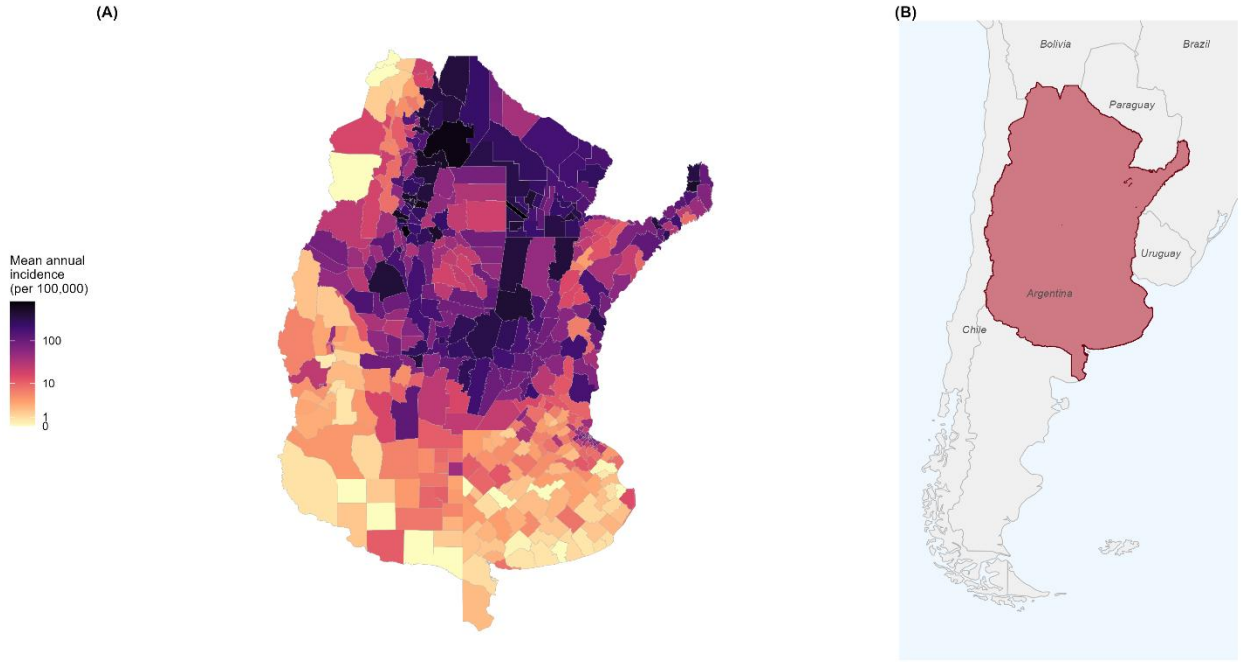
2. Methods

2.1 Study area and period

The study encompasses 473 departments across northern and central Argentina, spanning the period 2009–2025 (17 years). The region includes diverse ecological and socioeconomic conditions, ranging from

densely populated urban centres to rural agricultural zones, with varying levels of waste management infrastructure and healthcare access.

The geographic scope focuses on provinces where autochthonous dengue transmission has been documented: Jujuy, Salta, Formosa, Misiones, Chaco, Catamarca, Tucumán, Santiago del Estero, Santa Fe, Corrientes, La Rioja, Córdoba, San Juan, San Luis, Mendoza, La Pampa, and Buenos Aires (Figure 1). This delimitation balances two considerations. First, including southern temperate provinces — where transmission is largely climatically constrained — would introduce structural zeros, inflating zero-inflation beyond what disease dynamics alone produce. Second, restricting the analysis to historically endemic areas would exclude the expanding transmission frontier where prevention planning is most critical. The selected boundary approximates the southern limit of established *Ae. aegypti* populations documented through entomological surveillance [9], thereby capturing both endemic zones and recently colonized areas while excluding regions where only imported cases occur.



[FIGURE 1: Study area. (A) Mean annual dengue incidence per 100,000 by department of interest, 2009–2025; (B) location of the study area within Argentina, showing neighboring countries.]

2.2 Data sources

2.2.1 Epidemiological data

Dengue case data were obtained from the National Health Surveillance System (SNVS 2.0) of the Argentine Ministry of Health, aggregated by year and department of patient residence. Data for 2018–2025 are openly available through the national open-data portal [34], and records for 2009–2017 were compiled and kindly provided by M. Mauriño and F. Chesini. The SNVS 2.0 integrates mandatory notifications from all healthcare providers — including public hospitals, municipal health centers, primary care posts, and private-sector facilities and social-security providers — under the framework established by Law No. 15,465 on Notifiable Events (Eventos de Notificación Obligatoria). Cases span all age groups and both sexes. The SNVS records cases by classification (autochthonous, imported, or under investigation); because autochthonous transmission accounts for the large majority of reported cases (approximately 90% nationally in recent epidemic seasons) and the department-level aggregated data used here do not permit systematic exclusion of imported cases, all notified cases are included in the analysis. The outcome variable is the annual count of reported dengue cases per department, modelled with the expected count as an offset; incidence per 100,000 is reported for descriptive purposes only. Population denominators were derived from WorldPop high-resolution (~1 km) gridded population estimates [35, 36], aggregated to the department level by summing pixel counts within department boundaries for each year, avoiding the need to interpolate between census years. As in most endemic countries, surveillance relies predominantly on passive case detection through health facilities and is subject to substantial underreporting: published expansion factors for the Americas suggest that only a fraction of symptomatic infections are captured by routine surveillance, with reporting completeness varying by disease severity, healthcare access, and local diagnostic capacity, and further declining during large outbreaks when health systems become saturated [32, 33].

2.2.2 Climatic covariates

Climatic variables were extracted from ERA5 reanalysis [37] (0.25° resolution) and aggregated to the department level over two windows motivated by the seasonal life-cycle of *Aedes aegypti* and the cumulative nature of carry-over effects on vector populations: the current transmission season (January–April of year t) and the previous spring (September–December of year t−1). From these we derived current-summer temperature, relative humidity and precipitation, and lagged spring temperature and precipitation; relative humidity was computed from ERA5 temperature and dewpoint via the August–Roche–Magnus formulation [38]. Full variable definitions and sources are given in Table 1.

El Niño–Southern Oscillation

To capture inter-annual climate variability, each year was classified according to the dominant ENSO phase during the dengue transmission season (January–April), using a binary El Niño indicator (1 = El Niño year; 0 = La Niña or neutral year). Classification followed documented ENSO events (NOAA Climate Prediction Center [39]), identifying 2009, 2010, 2015, 2016, 2019, 2020, 2023 and 2024 as El Niño years within the study period.

2.2.3 Environmental and Land Cover Covariates

Land cover variables were derived from ESA Climate Change Initiative (CCI) land cover maps at 300 m resolution [40]: forest cover, agricultural land, and urban cover, each expressed as the proportion of department area. Annual maps were used when available (2009-2020) and extrapolated for the following years.

2.2.4 Waste management infrastructure

Exposure to waste-associated breeding habitats was quantified as the percentage of the department population residing within 500 m of official waste-disposal sites (landfills, open dumps, or recycling centers), calculated using population-weighted Euclidean distance buffers around georeferenced site locations obtained from provincial environmental agencies. A 500 m buffer was selected to reflect the limited flight range of *Ae. aegypti*, which typically disperses only short distances from breeding sites [41].

This variable serves as a proxy for proximity to artificial water-holding containers (discarded tires, plastic containers, cans) that provide ideal larval habitat [29].

2.2.5 Sociodemographic and infrastructural covariates

Sociodemographic and infrastructural indicators were obtained from national census data [42], with inter-census years interpolated linearly. These included the Unsatisfied Basic Needs index (NBI), which captures the proportion of households with unmet basic needs across dimensions of housing quality, sanitation, schooling, and economic capacity; a health vulnerability index reflecting healthcare-system fragility at the department level, where higher values indicate lower system capacity and access; and household piped-water coverage, defined as the percentage of households with piped water inside the dwelling and used here as a marker of water-supply infrastructure and, indirectly, of urbanization and household water-storage practices.

2.2.6 Post-pandemic indicators

A post-pandemic period indicator was additionally defined as an ordinal variable with three levels to capture the structural shifts in surveillance, mobility, and viral dynamics following the COVID-19 pandemic: 0 = pre-pandemic baseline (year < 2020), 1 = pandemic disruption year (year = 2020), 2 = post-pandemic regime (year > 2020). This ordinal coding separates the transition year from the sustained post-pandemic surveillance regime, which is more biologically and operationally plausible than a single binary cut.

Table 1 summarizes all candidate covariates and their sources.

Covariate	Definition	Spatial resolution	Temporal resolution	Source
Summer temperature	Mean daily T, Jan–Apr (°C)	0.25° (~28 km)	Monthly	ERA5 [37]
Summer rel. humidity	Mean RH, Jan–Apr (%)	0.25° (~28 km)	Monthly	ERA5; Lawrence [38]

Covariate	Definition	Spatial resolution	Temporal resolution	Source
Summer precipitation	Cumulative rainfall, Jan–Apr (mm)	0.25° (~28 km)	Monthly	ERA5
Lagged spring T / precip.	Mean T / cumulative rain, Sep–Dec, year t−1	0.25° (~28 km)	Monthly	ERA5
Land cover (forest/urban/agri.)	Proportion of department area (%)	300m	Annual	ESA CCI [40]
Waste-site proximity	% population within 500 m of disposal sites	Point locations	Static	Provincial agencies
Piped-water coverage	% households with in-dwelling piped water	Department	Decadal (2010, 2022)	INDEC census
Population density	Inhabitants per km²	~1km	Annual	WorldPop
NBI / health vulnerability	Sociodemographic indicators	Department	Decadal (2010, 2022)	INDEC census
El Niño phase	Binary indicator of El Niño transmission season	National/Global	Annual	NOAA CPC; Trenberth [39]
Post-pandemic period	Ordinal indicator (0/1/2): pre-2020, 2020, post-2020	—	Annual	—

Table 1: Candidate covariates evaluated in the model, with definitions and data sources.

2.3 Statistical analysis

2.3.1 Modeling framework

Dengue incidence was modeled using a Bayesian hierarchical regression within the Integrated Nested Laplace Approximation (INLA) framework [43]. INLA provides a computationally efficient approximation of Bayesian inference for latent Gaussian models and is particularly well-suited to disease mapping, where strong spatial and temporal dependence, excess zeros, and the need for full uncertainty quantification make a Bayesian hierarchical approach both natural and advantageous [44]. The general structure is:

$$Y_{it} \sim F(\mu_{it})$$

$$g(\mu_{it}) = log(E_{it}) + \beta_0 + \Sigma \beta_k X_{kit} + u_i + v_i + \gamma_t + \delta_{it}$$

where $F(.)$ represents any distribution (e.g. Poisson, negative binomial) ; $g(.)$ is the link function ; $_{it}$ is the observed case count in department i during year t ; E_{it} is the expected count (population × overall incidence rate) serving as an offset; β_k are fixed-effect coefficients for standardized covariates; u_i and v_i are spatially structured (intrinsic conditional autoregressive model; ICAR) and unstructured (independent and identically distributed; IID) random effects combined via the BYM2 parameterization [45]; γ_t is a temporally structured random effect; and δ_{it} is an IID space–time interaction term.

2.3.2 Distribution family selection

Four candidate distributions were compared to account for overdispersion and excess zeros: Poisson, negative binomial (NB), zero-inflated Poisson (ZIP), and zero-inflated negative binomial (ZINB). Comparison used the Watanabe–Akaike Information Criterion (WAIC).

2.3.3 Spatio-temporal structure

Spatial dependence was modeled using the BYM2 specification [45], which decomposes spatial variation into a spatially structured ICAR component and an unstructured IID component. The BYM2 reparameterization scales the precision matrix for prior transferability, assigns interpretable hyperparameters (precision τ and mixing parameter $\varphi \in [0,1]$, the proportion of variance that is spatially structured), and facilitates penalized complexity (PC) priors [46]. Neighborhood structure used queen

contiguity; isolated departments were connected to their two nearest neighbors by centroid distance to ensure a connected graph.

Temporal dependence was selected by WAIC from three alternative specifications fitted within the full structure (BYM2 + temporal + IID interaction): first-order random walk (RW1), second-order random walk (RW2), and first-order autoregressive (AR1).

2.3.5 Prior specification

Penalized complexity (PC) priors [46] were assigned to all random-effect hyperparameters, favoring simpler base models unless the data support additional complexity. For the spatial precision of the BYM2 component and the temporal precision of the RW1 effect, $P(\sigma > 1) = 0.01$; for the precision of the RW2 smooth and the IID space–time interaction, $P(\sigma > 0.5) = 0.01$; and for the BYM2 mixing parameter, $P(\varphi < 0.5) = 0.5$. Fixed-effect coefficients were assigned the default INLA Gaussian prior (mean 0, precision 0.001).

2.3.6 Covariate preprocessing

Continuous covariates were standardized (z-score) prior to modeling to facilitate comparison of effect magnitudes and improve numerical stability, and back-transformed to original scales for interpretation. Variables with >30% missing values were excluded.

2.3.7 Model Selection Procedure

Model building proceeded in four stages: (1) distribution-family selection on a reference spatio-temporal structure; (2) structure selection across nested random-effect specifications combining BYM2 spatial effects with RW1, RW2, or AR1 temporal effects, with and without an IID space–time interaction; (3) forward variable selection by WAIC improvement (threshold $\Delta\text{WAIC} > 2$); and (4) non-linearity assessment comparing linear and RW2 specifications for each selected continuous covariate (threshold $\Delta\text{WAIC} > 5$).

In addition to variables retained by forward selection, El Niño and post-pandemic period indicators were included as a priori theoretical covariates, given the established literature linking ENSO to dengue transmission in South America [22, 23] and the importance of disentangling ENSO from seasonal climate covariates that may partially capture the same signal; the post-pandemic indicator adjusts for the structural break in surveillance and transmission around 2020. Theory-driven inclusion was deliberately restricted to these two indicators; all other covariates entered only through data-driven selection.

Multicollinearity was screened using Variance Inflation Factors (VIF) with iterative removal of variables exceeding VIF > 10 [47]. El Niño, post-pandemic and post-pandemic categorical indicators were excluded from VIF screening.

2.3.8 Model Validation

Model performance was evaluated through three complementary approaches aligned with prevention-oriented objectives:

- **Risk classification.** Observed and predicted department-year incidence values were each independently assigned to one of three risk categories (Low, Medium, High) using tertile thresholds derived from the distribution of non-zero observed incidence values. The ability of the model's predicted categories to recover observed categories was then assessed using sensitivity (true positive rate for high-risk detection), specificity (true negative rate), positive predictive value (PPV), and the area under the receiver operating characteristic curve (AUC).
- **Ranking.** Spearman's rank correlation coefficient (ρ) between observed and model-predicted incidence — computed across all department-year observations — assessed the model's ability to correctly rank departments by risk level, which is more directly relevant to resource prioritization than point predictions.
- **Temporal cross-validation.** A forward-chaining scheme with an expanding training window was used to assess out-of-sample performance. The initial training window was set to 2009–2016 (eight

years) to ensure that random-effect hyperparameters were identified on at least two complete epidemic-to-interepidemic transitions (the 2009 and 2016 outbreaks), avoiding instability of the temporal and space–time interaction precisions when calibrated on a single epidemic cycle. The model was then refitted iteratively to predict each subsequent year $t \in \{2017, \ldots, 2025\}$ using only data from years strictly preceding t. Unlike random k-fold cross-validation, this scheme prevents information leakage from future observations through the BYM2 spatial and space–time interaction random effects, making it the only honest assessment for a temporal surveillance application.

2.3.9 Risk Classification for Prevention Planning

For prevention planning purposes, departments were stratified into four priority tiers based on mean predicted incidence across the study period. Tier boundaries were defined using the same tertile thresholds as in Section 2.3.8, with the lower tertile further subdivided at its midpoint to distinguish Moderate from Low risk: Very High (≥ upper tertile threshold), High (≥ lower tertile threshold and < upper tertile threshold), Moderate (≥ 50% of the lower tertile threshold), and Low (< 50% of the lower tertile threshold). This four-tier scheme provides finer operational granularity than the three-class validation framework, distinguishing endemic core areas from transition zones and the emerging frontier. The top 20% of departments by predicted risk were additionally identified as priority targets for intensified surveillance and vector control.

2.3.10 Effect Interpretation

Fixed-effect coefficients were back-transformed from the standardized to the original scale and expressed as risk ratios. For a continuous covariate X with standard deviation SD(X), the back-transformation is:

$$\beta_{\text{original}} = \frac{\beta_{\text{standardized}}}{\text{SD}(X)}$$

$$\text{RR per unit} = \exp\left(\beta_{\text{original}}\right)$$

where $\beta_{\text{standardized}}$is the posterior mean coefficient on the *z*-score-scaled covariate, and RR per unitis the multiplicative change in expected incidence associated with a one-unit increase in X on its original scale. Risk ratios are reported with 95% credible intervals (CI); effects were considered significant when the CI excluded RR = 1.

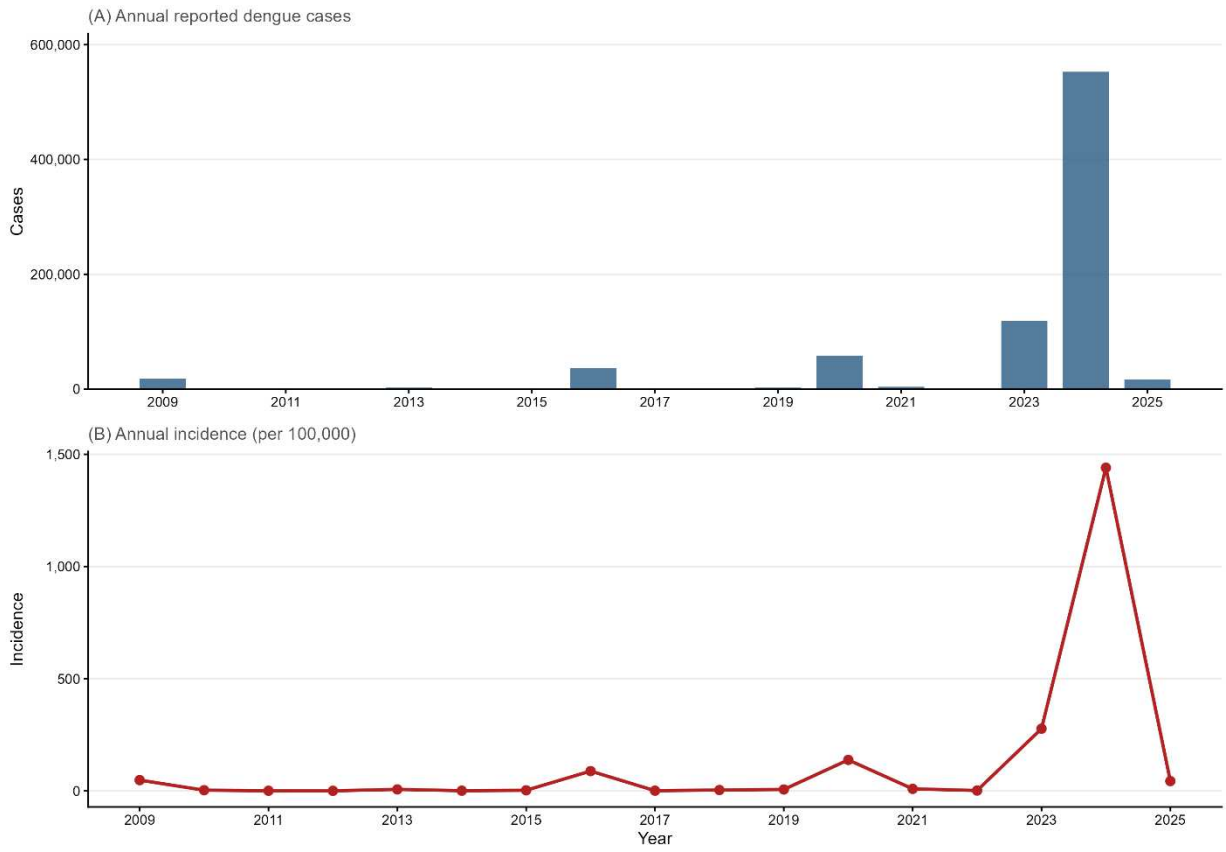
2.3.11 Software

Analyses were conducted in R 4.4.3 using *R-INLA*. Spatial data were handled with *sf* and *spdep*; visualizations used *ggplot2* and *patchwork*.

3. Results

3.1 Descriptive epidemiology

Over the 17-year study period (2009–2025), a total of 817,699 dengue cases were reported across 473 departments. Annual cases exhibited extreme variability, from a few hundred cases in inter-epidemic years (e.g., 229 in 2012) to a record exceeding 500,000 nationally in 2024 — approximately four-fold higher than the 2023 outbreak (Figure 2). The 2024 epidemic marks an inflection point in Argentina's dengue history, with transmission documented across an expanded geographic range including departments in temperate central provinces. The distribution of department-year counts is strongly right-skewed: 76.6% of observations recorded zero cases, reflecting both true absence of transmission in climatically marginal areas and underreporting where surveillance capacity is limited.



[FIGURE 2: Annual dengue cases (A) and incidence (per 100,000) (B), 2009–2025.]

3.2 Model selection

3.2.1 Distribution family

Four candidate distributions were compared on a reference spatio-temporal structure (BYM2 + AR1, three covariates). The zero-inflated negative binomial family had the lowest WAIC (22,729.2), marginally ahead of the negative binomial (22,730.0; ΔWAIC = 0.8 — within the noise of WAIC differences). Both substantially outperformed ZIP (1,149,454) and Poisson (1,310,969), which fail to accommodate the strong overdispersion in the data. The ZINB family was retained for the final model on both empirical and theoretical grounds, since 76.6% of observations are zeros and the dual zero-generating processes (structural absence and counting zeros from surveillance limitations) are biologically plausible. The

306 estimated zero-probability parameter of the ZINB component is small (posterior median ≈ 0.001),
307 confirming that the negative-binomial component does most of the modeling work while ZINB provides a
308 parsimonious safeguard for residual structural zero-inflation.

309 **3.2.2 Spatio-temporal structure**

310 Eleven random-effect structures were compared at the full set of candidate covariates (Table 2). The full
311 model combining BYM2 spatial effects, RW1 temporal effects, and an IID space–time interaction provided
312 the best fit (M7_Full_RW1: WAIC = 22,059.0). The AR1 alternative was distanced by ΔWAIC = 47.2 and
313 the more strongly smoothed RW2 by ΔWAIC = 69.1, indicating that the year-to-year structure is too
314 irregular for a second-order penalty or a single autoregressive coefficient. Models lacking the IID
315 interaction were substantially worse (ΔWAIC ≥ 618), confirming that dengue dynamics in Argentina are
316 not separable in space and time.

Model	Structure	WAIC	ΔWAIC
M7_Full_RW1 (selected)	BYM2 + RW1 + IID interaction	22,059.0	0
M8_Full_AR1	BYM2 + AR1 + IID interaction	22,106.1	+47.2
M7bis_Full_RW2	BYM2 + RW2 + IID interaction	22,128.1	+69.1
M6_ST_AR1	BYM2 + AR1	22,676.8	+617.8
M5_ST_RW1	BYM2 + RW1	22,678.5	+619.5
M2_Spatial	BYM2	23,942.3	+1,883.4
M4_Temp_AR1	AR1	24,743.2	+2,684.3
M3_Temp_RW1	RW1	24,754.4	+2,695.5
M3bis_Temp_RW2	RW2	24,826.6	+2,767.7
M1_Fixed	Covariates only	26,199.6	+4,140.7
M0_Null	Intercept only	27,694.9	+5,636.0

Table 2: Model structure comparison (WAIC) using the full candidate covariate set and the ZINB family. The selected model combines BYM2 spatial effects, an RW1 temporal trend, and an IID space–time interaction.

3.3 Covariate selection

3.3.1 Forward selection

Forward stepwise selection identified five covariates meeting the ΔWAIC > 2 threshold: the department-level health-vulnerability index, population within 500 m of waste-disposal sites, current-summer temperature, the previous-spring temperature, and current-summer relative humidity (Table 3). The cumulative WAIC reduction from forward selection was 63.0 units. The El Niño and post-pandemic indicators were subsequently included a priori on theoretical grounds, their joint inclusion produced a marginal WAIC degradation (ΔWAIC = +2.3), but the El Niño posterior risk ratio remained robust (Section 3.4) and its inclusion appears essential for disentangling ENSO from seasonal climate covariates. Population density, the NBI socioeconomic index, household piped-water coverage, land cover, and the candidate precipitation variables were evaluated but did not meet the selection threshold.

Table 3: Variable selection history. Steps 1–5 reflect forward selection by WAIC (ΔWAIC > 2; negative values denote WAIC reduction). The El Niño and post-pandemic indicators were added jointly a priori on theoretical grounds, despite a marginal WAIC degradation.

Step	Variable	WAIC	ΔWAIC
1	Health vulnerability index	22,709.7	−25.1
2	Population within 500 m of waste sites	22,699.4	−10.3
3	Summer temperature (Jan–Apr)	22,693.6	−5.8
4	Previous-spring temperature (Sep–Dec, t−1)	22,686.3	−7.3
5	Summer relative humidity	22,671.8	−14.5
6	El Niño phase (a priori) + post-pandemic (a priori)	22,674.1	+2.3

3.3.2 Non-linearity assessment

Each forward-selected continuous covariate was compared against an RW2 smooth specification (threshold ΔWAIC > 5). Only one of the five covariates exhibited strong evidence of non-linearity: the previous-spring temperature (ΔWAIC = −7.0), which was therefore retained as a smooth (RW2) effect in the final model. The remaining four covariates — the health-vulnerability index, waste-site proximity, current-summer temperature, and current-summer relative humidity — showed no meaningful improvement under the non-linear specification (all $|\Delta\text{WAIC}| < 4$) and were retained as linear effects on the log-risk scale. This separation is consistent with the biological intuition that the temperature of an extended antecedent window integrates threshold and saturation effects on vector build-up, whereas the contemporaneous thermal–hygric and socio-environmental terms act approximately monotonically within the ranges observed.

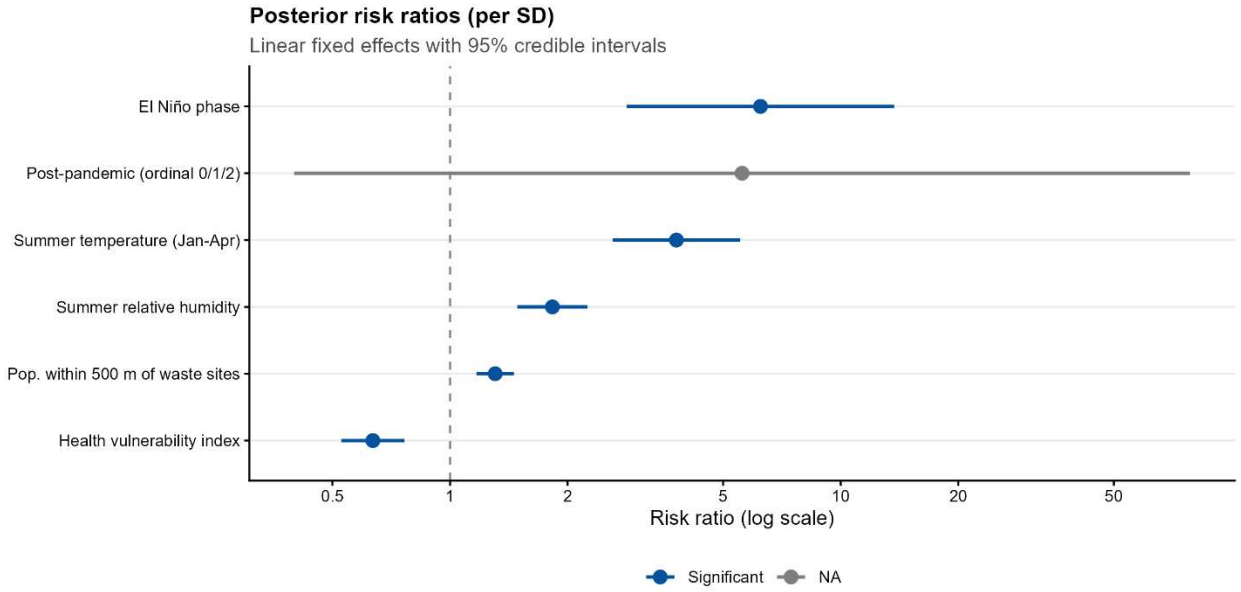
3.4 Fixed effects

The final model included six linear fixed effects (Table 4; Figure 3) and one non-linear smooth effect (Figure 4). Among the linear effects, five had 95% credible intervals (CI) excluding RR = 1; only the post-pandemic indicator was non-significant after adjustment. Effects are reported both per standard deviation (per Standard Deviation (SD), for comparing magnitudes) and per natural unit (per °C, per percentage point) on the original scale.

Variable	RR per SD	95% CI	RR per unit	95% CI (unit)
El Niño phase	6.23	[2.84, 13.70]	binary	—
Post-pandemic (ordinal 0/1/2)	5.59	[0.40, 78.38]	6.77 /level	ns
Summer temperature (Jan–Apr)	3.80	[2.61, 5.53]	1.41 /°C	[1.28, 1.55]
Summer rel. humidity	1.83	[1.49, 2.25]	1.06 /pp	[1.04, 1.08]
Pop. w/in 500 m of waste sites	1.30	[1.17, 1.46]	1.05 /pp	[1.03, 1.07]
Health vulnerability index	0.63	[0.53, 0.76]	composite	—

Table 4: Posterior fixed-effect estimates (linear terms). RR per SD reflects a one-standard-deviation increase; RR per unit is back-transformed to the original scale. pp = percentage point; ns = not significant. All listed effects except the post-pandemic indicator have 95% credible intervals excluding RR = 1. The previous-spring temperature is modeled as a smooth non-linear effect and presented separately below (Section 3.4.1).

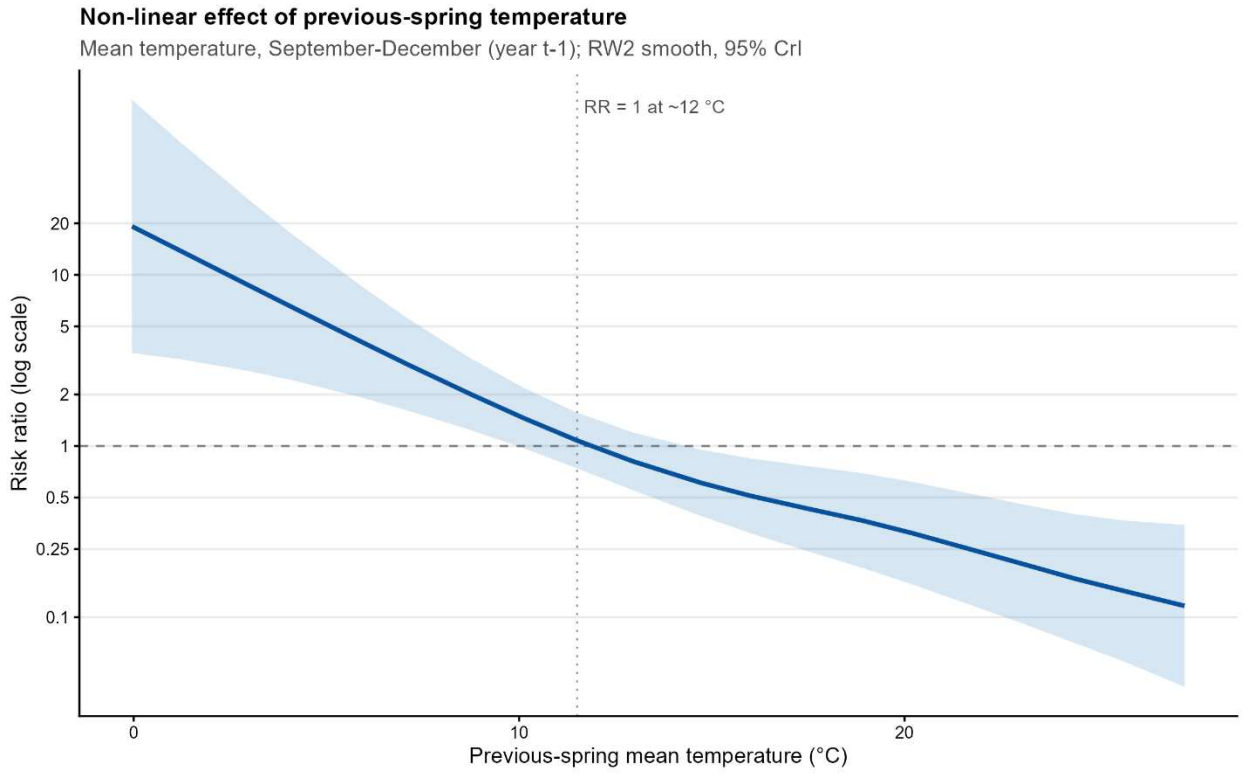
El Niño years carried by far the largest effect — a 6.2-fold increase in risk per standard deviation (RR per SD = 6.23; 95% CI: 2.84–13.70) — after adjustment for seasonal climate and socioeconomic covariates. Among contemporaneous climate variables, current-summer temperature (January–April) was the strongest linear predictor (RR = 1.41 per °C; 95% CI: 1.28–1.55), and current-summer relative humidity was independently associated with elevated risk (RR = 1.06 per percentage point; 95% CI: 1.04–1.08). Population residing within 500 m of waste-disposal sites was positively associated with risk (RR = 1.05 per percentage point; 95% CI: 1.03–1.07), whereas the department-level health-vulnerability index was inversely associated with reported incidence (RR per SD = 0.63; 95% CI: 0.53–0.76). The post-pandemic indicator had a large posterior mean (RR per SD = 5.59) but a credible interval crossing 1 (95% CI: 0.40–78.38).



[FIGURE 3 — Forest plot of linear fixed effects (per SD), NA = not significant]

3.4.1 Non-linear previous-spring temperature effect

The temperature of the previous spring (September–December, year t−1) exhibits a pronounced non-linear association with dengue risk (Figure 4, ΔWAIC = −7.0 in favour of the RW2 smooth). The relationship is monotonically decreasing across the observed range but with marked curvature: posterior risk ratios fall from RR ≈ 19 at the coldest previous springs (≈ 0 °C) to RR ≈ 0.1 at the warmest (≈ 27 °C), crossing RR = 1 near 11–13 °C, with the steepest change concentrated at the cold end of the range. The 95% credible interval excludes RR = 1 at both ends of the distribution — cold previous springs being associated with elevated subsequent risk and warm previous springs with reduced risk — while the interval widens markedly towards the sparsely populated extremes of the temperature range.



[FIGURE 4: Non-linear effect of previous-spring temperature (September–December, year t−1) on dengue risk (RW2 smooth) with 95% credible interval. Risk decreases monotonically with warmer antecedent springs, crossing RR = 1 near 11–13 °C.]

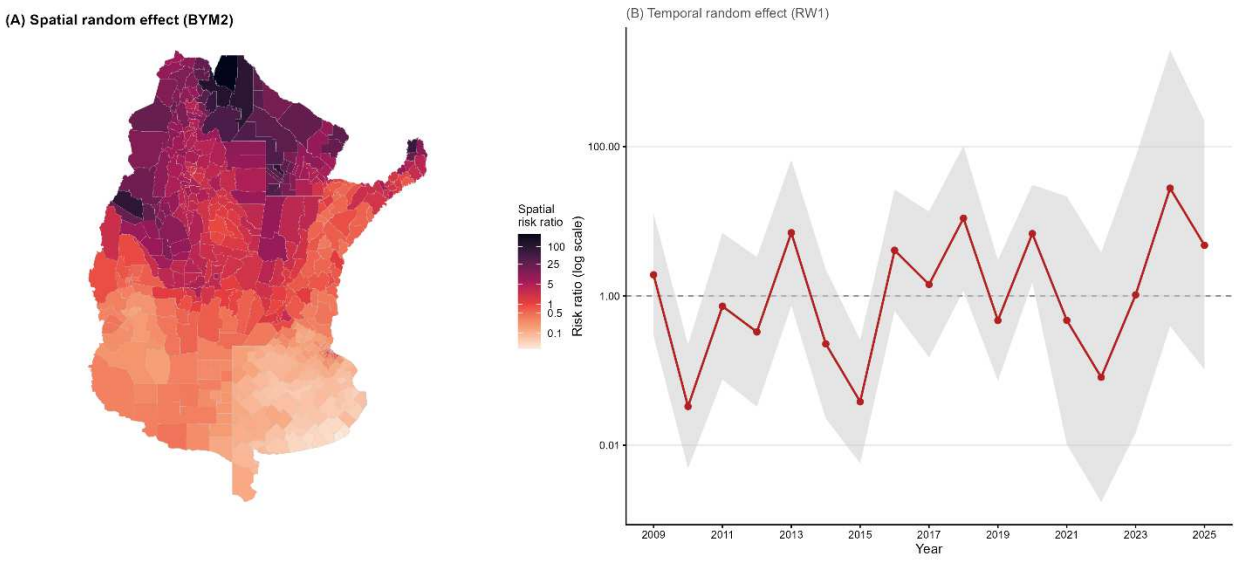
3.5 Random effects

3.5.1 Spatial random effects

The BYM2 spatial component revealed pronounced geographic clustering (mixing parameter $\varphi = 0.960$; 95% CI: 0.846–0.998), indicating that most of the spatial variance is spatially structured rather than independent across departments. The precision parameter ($\tau_space = 0.78$; 95% CI: 0.61–0.99) corresponds to substantial residual spatial heterogeneity after accounting for measured covariates. The spatial risk surface shows a clear north-east to south-west gradient: residual risk is highest in north-eastern departments bordering Brazil and Paraguay (the historical endemic core) and declines progressively towards the southern and western departments approaching the transmission frontier (Figure 5A).

3.5.2 Temporal random effects

The RW1 temporal component captures inter-annual variability remaining after adjustment for the fixed effects, including the El Niño and post-pandemic indicators (Figure 5B). Substantial residual temporal variation persists, with elevated random effects in years of intense transmission — most strikingly 2024 (RR ≈ 27.7), which retains by far the highest temporal risk ratio even after accounting for the El Niño event — and suppressed effects during inter-epidemic lulls (2010: RR ≈ 0.03; 2015: RR ≈ 0.04). Wide credible intervals throughout reflect the inherent difficulty of characterizing rare epidemic events with limited replication. The persistence of a strong residual temporal signal indicates that meaningful inter-annual variation is not fully captured by the measured drivers, plausibly reflecting viral introduction events, serotype dynamics, and population-immunity cycling.



[FIGURE 5: Estimated random effects. (A) Spatial random effect (BYM2): department-level residual risk ratios; (B) Temporal random effect (RW1): year-specific risk ratios on a log scale with 95% credible intervals.]

3.5.3 Space–time interaction

The IID space–time interaction (τ_{st} = 0.52; 95% CI: 0.43–0.61) captured department-year-specific variation not explained by additive spatial and temporal effects. Its substantial variance confirms that dengue dynamics in Argentina are not separable in space and time: epidemic waves affect different geographic areas to different extents in different years.

3.6 Model validation

3.6.1 In-sample risk classification

The model achieved outstanding in-sample discrimination between high-risk and low/medium-risk department-years (AUC = 0.99; sensitivity 91.9%, specificity 98.0%). In-sample metrics reflect descriptive fit and are not interpreted as evidence of out-of-sample predictive skill.

3.6.2 Forward-chaining cross-validation

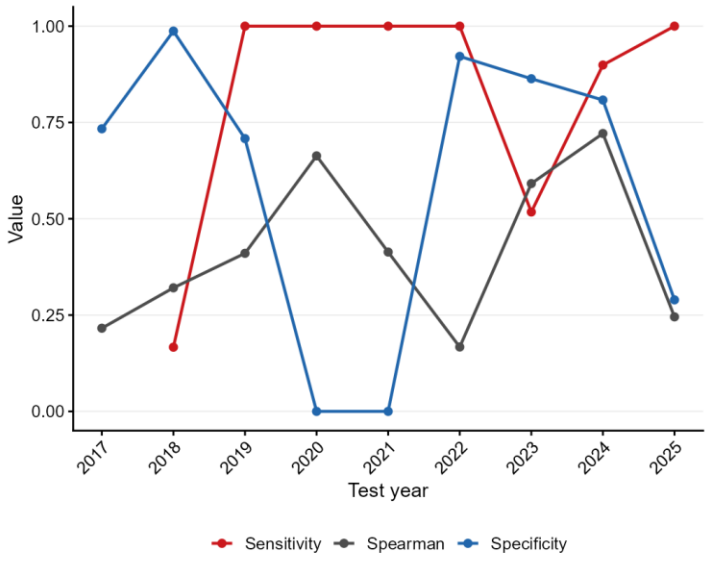
Forward-chaining temporal cross-validation provided a realistic estimate of out-of-sample performance across nine test years (2017–2025; Table 5). The initial eight-year training window (2009–2016) ensured that random-effect hyperparameters were calibrated on at least two complete epidemic-to-interepidemic transitions before any out-of-sample prediction was attempted. Pooled classification skill remained useful for surveillance purposes (cross-validated sensitivity 83.2%, specificity 57.6%, Spearman $\rho = 0.40$), though substantially below the optimistic estimates that random k-fold CV would yield in this setting. Pooled predictive metrics based on absolute case counts (RMSE, R^2) are dominated by a small number of folds where the epidemic magnitude exceeded anything observed during training. The clearest example is 2020–2021: when the model was trained exclusively on pre-pandemic data and asked to predict the post-pandemic surveillance and transmission regime, it systematically over-predicted case counts in absolute terms, driving RMSE and R^2 to extreme values that reflect this structural regime shift rather than a general failure of spatial risk discrimination. We therefore report Spearman ρ and per-fold classification metrics as the meaningful summaries.

Metric	Value
Cross-validated sensitivity	83.2%
Cross-validated specificity	57.6%
Cross-validated PPV	22.7%
Cross-validated Spearman ρ	0.40
Cross-validated 95% CI coverage	31.1%

Table 5: Model performance. Cross-validation uses a forward-chaining expanding-window design over nine test years (2017–2025), with an eight-year initial training window (2009–2016) ensuring identification on two complete epidemic-to-interepidemic transitions. Pooled RMSE and R^2 are omitted as they are dominated by extreme extrapolation artifacts in single folds. PPV = positive predictive value.

3.6.3 Per-Fold performance

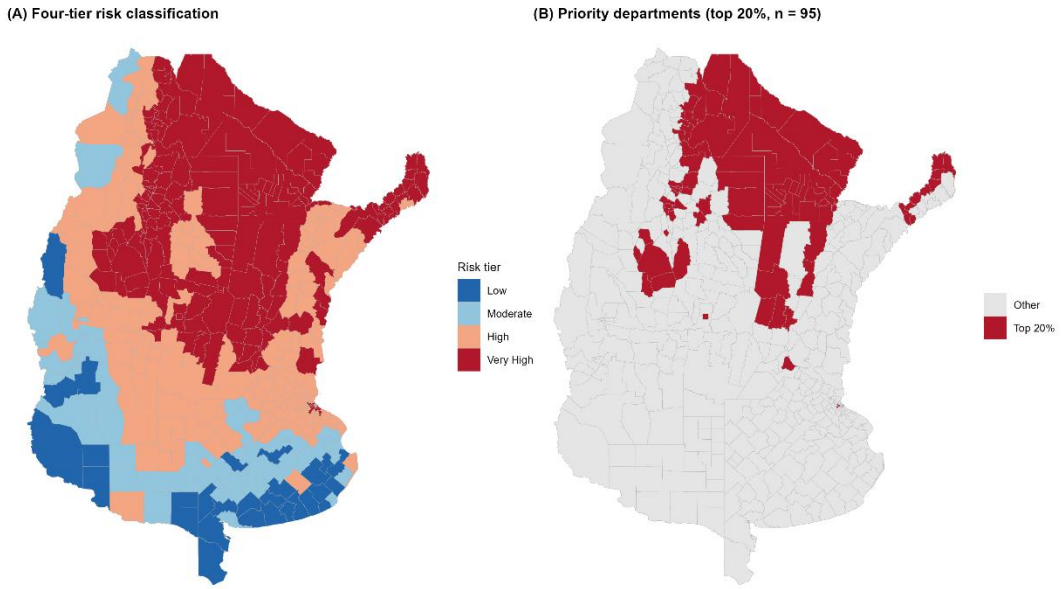
Per-fold metrics (Figure 6) show that the model performs best for the most recent and largest epidemics: 2024 (sensitivity 89.9%, specificity 80.8%, positive predictive value 91.3%, Spearman ρ = 0.72) and 2023 (sensitivity 51.8%, specificity 86.4%, PPV 54.6%). Predictive performance is weakest for the 2020–2021 folds, where the post-pandemic regime had not yet been observed at training time and the model over-predicted high-risk classification almost universally (false-positive rates close to 1 in those two years). This pattern is consistent with the model's design objective: it stratifies spatial risk reliably once the epidemic regime is observed and degrades gracefully when forecasting into unprecedented conditions. The 2024 fold — the largest and most consequential epidemic in the study period, taking place under conditions broadly comparable to the post-pandemic regime already observed during 2022–2023 — is precisely the type of event for which the model is most useful: it identified about 90% of the high-risk department-years correctly with a positive predictive value of 91%, demonstrating operationally relevant performance under conditions that resembled the recent training experience.



[FIGURE 6: Per-fold metrics: Sensitivity, Specificity and Spearman observed vs. predicted correlation.

3.7 Risk stratification for prevention

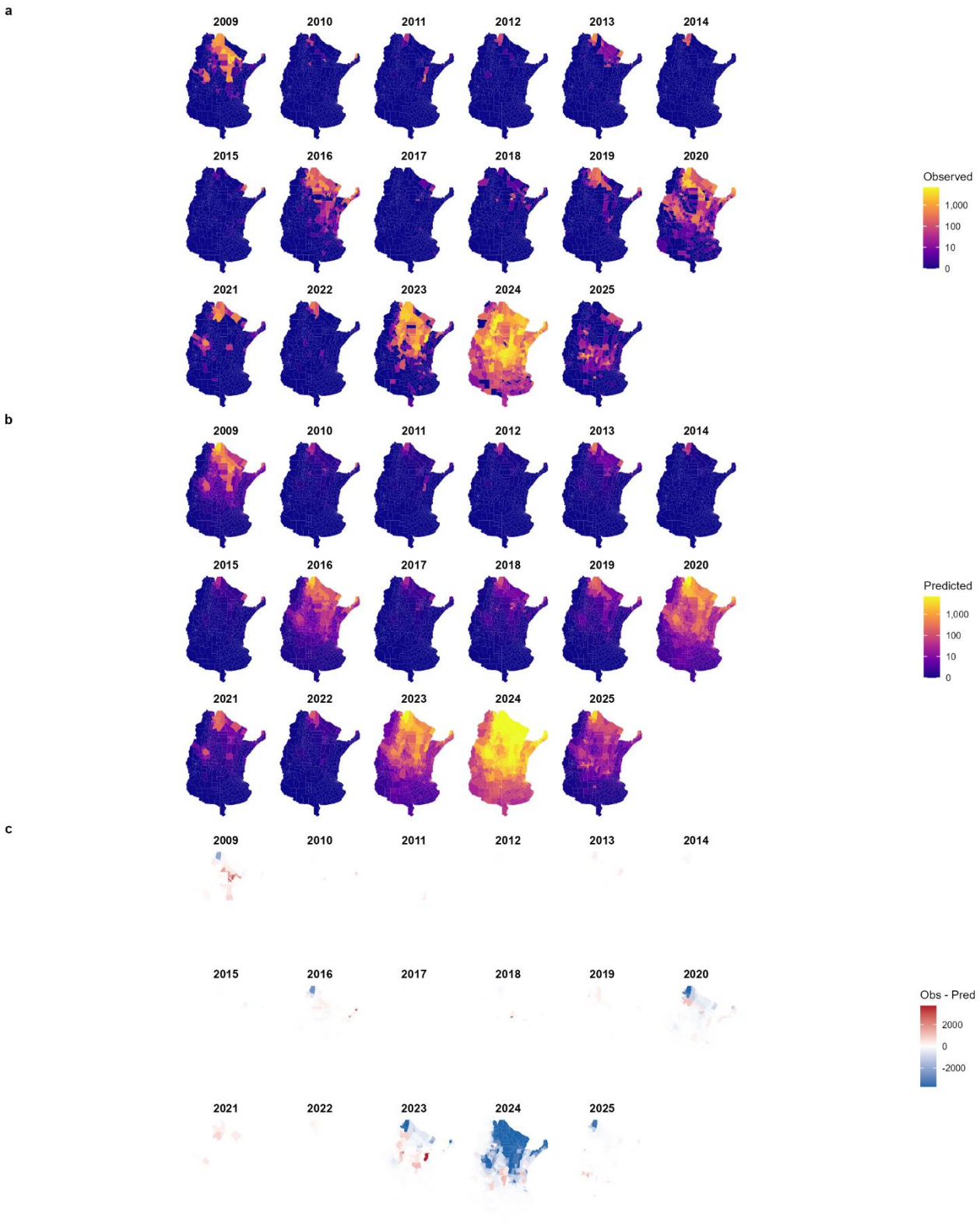
Departments were stratified into four priority tiers based on mean predicted incidence (Figure 7). The top 20% of departments by predicted risk accounted for approximately 66.0% of total cases over the study period, demonstrating efficient resource targeting through spatial risk stratification. Very-high-risk departments concentrated in the northern endemic core, while transition zones and the southern frontier formed lower tiers.



[FIGURE 7: (A) Dengue risk classification map (four tiers); (B) priority departments (top 20% by predicted risk).]

3.8 Spatio-temporal patterns

Year-by-year mapping of observed and predicted incidence revealed distinct epidemic waves affecting different geographic areas over time (Figure 8). The model reproduced the spatial expansion of transmission during epidemic years while maintaining stable estimates for endemic areas. Prediction residuals concentrated in epidemic years and along the southern transmission frontier, where epidemic expansion has been most dynamic and least predictable.


a
2009
2010
2011
2012
2013
2014
2015
2016
2017
2018
2019
2020
2021
2022
2023
2024
2025
Observed
1,000
100
10
0
b
Predicted
1,000
100
10
0
c
Obs - Pred
2000
0
-2000

459

[FIGURE 8: Spatio-temporal maps of dengue incidence (cases/100000 inhab.) by year. (A) Observed; (B) Predicted; (C) Residuals (observed − predicted).]

4. Discussion

This study provides a comprehensive spatio-temporal analysis of dengue risk factors and spatial patterns across Argentina's endemic and emerging transmission zones over 2009–2025, a period that includes the country's largest recorded epidemic. The Bayesian hierarchical framework is well-suited to this setting, simultaneously accommodating spatial and temporal dependence, excess zeros, and full uncertainty quantification. Five principal findings emerge.

First, the El Niño–Southern Oscillation is the leading inter-annual driver of dengue risk in Argentina, with El Niño years associated with a 6.2-fold increase in risk after adjustment for seasonal climate and socioeconomic covariates. This finding aligns with a growing body of evidence linking ENSO to dengue across the Americas: Stewart Ibarra et al. [22] documented ENSO modulation of transmission in coastal Ecuador, Lowe et al. [23] reported similar effects in Barbados, Vincenti-Gonzalez et al. [21] demonstrated ENSO-driven periodic outbreaks in Venezuela, and Anyamba et al. [24] provided a hemispheric analysis linking the 2015–2016 El Niño to *Aedes*-borne disease surges. The persistence of the ENSO effect after adjustment for current-summer and antecedent-spring climate variables indicates that it captures inter-annual variability beyond mean seasonal conditions — reflecting rainfall timing, the persistence of favorable conditions across consecutive seasons, and multi-year vector dynamics [25, 27]. Because ENSO indices are forecastable months ahead, this result has direct operational value for early warning.

Second, current-summer thermal–hygric conditions are the dominant intra-seasonal climatic drivers. The summer temperature effect (41% increase per °C) is consistent with mechanistic models identifying a transmission optimum near 29 °C [19] and is comparable to the upper range reported by Brazilian and Caribbean Bayesian spatio-temporal analyses [23, 48]. The substantial magnitude in our data

plausibly reflects the inclusion of expanding transmission frontiers, where small increases in mean summer temperature translate into a step-change in transmission suitability. The independent positive effect of summer relative humidity (6% per percentage point) complements the temperature result: humidity governs adult vector survival, biting behavior, and the extrinsic incubation period through pathways distinct from temperature [21, 49]. Together, these results indicate that compound heat-and-humidity anomalies — expected to become more frequent under climate change — will progressively expand the geographic and seasonal extent of transmission.

Third, the previous-spring temperature carries a carry-over signal into the following transmission season. Colder previous springs (September–December of year $t-1$) were associated with higher subsequent risk, the RW2 smooth declining from elevated values at cool antecedent springs toward lower risk at warmer ones and crossing RR = 1 near 11–13 °C (Figure 4). The curvature is the most robust feature of this effect; the extreme RR values at the tails of the temperature distribution (RR ≈ 19 at the coldest and RR ≈ 0.1 at the warmest antecedent springs) carry wide credible intervals owing to data sparsity and should be read with caution.

To our knowledge, this is the first explicit demonstration of a non-linear antecedent-spring temperature effect in a dengue spatio-temporal model for subtropical South America. We present it as a robust empirical signal and favour a reading that integrates two complementary biological pathways. The first is water-centred: to the extent that a cooler-than-usual previous spring coincides with a drier pre-season, a well-established mechanism links antecedent dryness to later dengue through domestic water storage — where piped supply is unreliable, households respond to water scarcity by storing water in containers that become prime larval habitat, translating drought into elevated risk months later [30, 31, 50]. This delayed pathway has been quantified directly in Barbados, where drought raised dengue risk at lead times of up to five months through exactly this mechanism [23]. The second pathway operates through the egg bank: recent work on temperate Argentine *Ae. aegypti* populations has shown that short-photoperiod conditions induce diapause-related responses in eggs, including increased cold tolerance, higher lipid reserves, and delayed hatching

that can buffer populations across unfavourable seasons [51, 52, 53]. A cooler, shorter previous spring could therefore limit the size and viability of the overwintering egg bank that seeds the following season's vector population — a mechanism distinct from, but complementary to, the water-storage pathway. On this combined reading, the previous-spring temperature acts partly as a proxy for a dry, storage-prone pre-season and partly as a modulator of egg-stage overwintering success, rather than as a direct thermal effect on adult vectors.

Latitude is a second, equally important consideration. Previous-spring temperature is strongly structured by latitude and climatic zone, and although the BYM2 spatial random effect absorbs the stable south-to-north gradient in mean risk, residual latitudinal and climatic-zone structure may still be channelled through this covariate. The study area spans the southern, cold-limited distributional fringe of *Ae. aegypti* [9, 10], where antecedent thermal conditions co-vary tightly with the length and intensity of the favourable season, so a purely climatic interpretation cannot be separated cleanly from this underlying geographic gradient. We therefore read the effect cautiously: disentangling genuine antecedent dryness/water-storage and egg-bank effects from residual latitudinal confounding will require finer-scale, anomaly-based exposures — for example a standardised precipitation index for the previous spring — paired with stage-specific entomological monitoring.

Fourth, sociodemographic and infrastructural factors contribute measurable and partly modifiable risk. The positive association between waste-site proximity and dengue risk extends entomological observations of elevated *Ae. aegypti* densities near waste-disposal sites [29] to the population-health scale across an entire national dataset; the use of a 500 m buffer aligns the exposure metric with the vector's short dispersal range [41].

The inverse association between the health-vulnerability index and reported incidence warrants careful interpretation and becomes coherent once it is recalled that the outcome is reported cases. Departments with lower health-system vulnerability — that is, better health infrastructure and access — are precisely those

best able to detect, confirm, and report dengue, so a lower vulnerability score is expected to translate into more reported cases. This mechanism is well documented for vector-borne diseases modelled from routine surveillance data: passive case detection systematically under-captures cases in areas with poor healthcare access, generating apparent inverse associations between infrastructure quality and reported incidence that reflect ascertainment gradients rather than genuine protective effects [54]. The index therefore plausibly operates in two reinforcing ways: as a proxy for urbanization, with its attendant population density, container abundance, and transmission intensity; and as a marker of ascertainment capacity that highlights the underreporting likely to affect the most vulnerable, least-resourced departments. This dual reading — rather than any protective effect of vulnerability itself — is the most parsimonious account of the observed gradient, and it underscores both the limits of ecological inference and the importance of accounting for surveillance heterogeneity when interpreting models built on reported cases.

Fifth, the model excels at spatial risk classification but degrades when extrapolating epidemic magnitude. Forward-chaining cross-validation confirmed that the model reliably identifies high-risk departments (pooled sensitivity 83.2%) and produces a moderate but meaningful ranking of departments by risk (Spearman $\rho = 0.40$ pooled), a level of discrimination consistent with what has been reported in comparable dengue spatio-temporal models in the region. The 2024-fold, the largest and most consequential epidemic in the study period, was identified with operational accuracy (sensitivity 89.9%, PPV 91.3%): predictions in that year were already drawing on a training experience that included the comparable 2023 outbreak, so the model could anchor its priors in observed conditions.

The divergence of pooled RMSE in some folds reflects the inability to extrapolate epidemic magnitudes beyond the historical range — most acutely for 2020–2021. This poor fit during the pandemic period is not surprising: COVID-19 exerted complex, countervailing effects on dengue dynamics that are difficult to capture with a simple ordinal indicator. Mobility restrictions and social distancing likely reduced human–vector contact and transmission intensity, while simultaneously depressing healthcare-seeking behaviour and thus increasing underreporting of cases that did occur — two opposing signals that partially cancel out

in reported incidence data [55]. These effects were concentrated in 2020 and the immediate transition year, which may explain why the three-level post-pandemic indicator — which conflates the acute disruption year with the sustained post-pandemic regime — is poorly identified in the model after adjustment for El Niño and the RW1 temporal effect. This divergence is consistent with difficulties reported in other dengue forecasting efforts [48] and reflects the fundamental challenge of forecasting non-stationary epidemic processes where structural breaks in both transmission and surveillance occur simultaneously. For prevention planning, classification skill is the more actionable property: resources can be allocated to consistently high-risk areas without accurate case-count forecasts.

4.1 Limitations

Several limitations warrant consideration. First, surveillance relies on passive case detection through public and private healthcare facilities — though the SNVS 2.0 legally requires notification from both sectors, completeness of private-sector reporting in practice remains variable — and is subject to underreporting that varies spatially with healthcare access and, during large outbreaks, with health-system strain: when reporting capacity is exceeded, additional cases within already-diagnosed households may go unreported without formal clinical confirmation, compounding ascertainment bias. The introduction of dengue vaccination (Qdenga) in some provinces (notably Salta and Misiones from 2024) will further alter both transmission and reporting dynamics and should be incorporated in future analyses. Second, the El Niño indicator is a binary simplification of a continuous phenomenon; continuous ENSO indices (e.g., the Oceanic Niño Index) could capture intensity gradients, and the classification of transition years involves judgment. Third, the post-pandemic ordinal indicator is poorly identified after adjustment for El Niño and the RW1 temporal effect, with a credible interval crossing one; it should be interpreted as a coarse baseline adjustment rather than a substantive estimate. Fourth, the cross-validated credible-interval coverage of approximately 31% indicates that the model is overconfident in its posterior predictive intervals — a well-known limitation when combining strong shrinkage priors with sparse-count data [56]. To mitigate this, PC

priors on precision parameters were specified to regularize random-effect variances, and the forward-chaining validation scheme was designed to avoid artificially narrow intervals from information leakage; residual overconfidence remains a target for future work using wider priors or a posterior calibration step. Fifth, the waste-site and socio-environmental variables are measured at the department level, which is coarsely relative to the fine spatial scale of dengue transmission; in particular, micro-scale waste accumulation within cities and household-level container availability — major drivers in practice — are not captured at this resolution. Intra-urban analyses at finer scales have documented substantial within-city heterogeneity in *Ae. aegypti* breeding-site distribution in Argentine cities [57, 58] and are needed to translate the national-scale patterns identified here into targeted local interventions. Sixth, the previous-spring temperature effect, while robust in our analysis, is identified at the department-level scale and is correlated with latitude and climatic zone; its interpretation as a vector-phenology signal via egg-bank overwintering [51, 53] rather than residual spatial confounding remains provisional, and future work pairing entomological monitoring with the climatic exposure quantified here would strengthen causal inference. Seventh, several potentially relevant covariates (e.g., human mobility, serotype circulation, vector-control intensity) could not be included for lack of consistent department-level data. Finally, an alternative parameterization using ENSO as a temporal structural component (rather than a fixed-effect covariate) was considered; the chosen specification preserves the flexibility of the RW1 temporal effect to absorb residual inter-annual variability not directly attributable to ENSO (immunity cycling, serotype dynamics, surveillance change) while explicitly quantifying the ENSO contribution.

4.2 Implications for prevention planning

Our results translate into concrete implications. The strong, forecastable ENSO effect supports the development of a seasonal-scale dengue early warning system in which El Niño forecasts entering the spring–summer transition could trigger resource pre-positioning, intensified vector control, reinforced clinical surveillance, and the prioritization of vaccination campaigns in high-risk areas — particularly

relevant given the recent introduction of Qdenga in some Argentine provinces. The strong antecedent-spring temperature signal extends this early-warning horizon further upstream: by the end of the austral spring (December), the antecedent thermal regime is already known and could feed an additional predictive signal complementing the ENSO forecast and providing several months of lead time before the peak of transmission. The dominance of current-summer thermal–hygric conditions confirms January–April as the critical operational window for intensified surveillance and response. The persistent waste-site association highlights waste management — including the micro-scale dumping sites and household containers that operate below the resolution of this analysis — as a modifiable target; improved waste collection and container removal in high-exposure areas could reduce breeding habitat availability. Spatially, the top 20% of departments account for the large majority of cases, enabling efficient resource targeting, while the documented southward expansion — evident in the 2024 epidemic reaching central provinces — argues for an expanded surveillance footprint that anticipates the transmission frontier rather than reacting to it. Within priority areas, household water storage practices and micro-scale waste accumulation merit attention as locally actionable determinants of vector productivity.

5. Conclusions

Bayesian spatio-temporal modeling can effectively stratify dengue risk across Argentina's heterogeneous transmission settings, even when forecasting outbreak magnitude remains challenging. Inter-annual climate variability driven by ENSO emerges as the leading determinant of dengue risk — alongside current-summer temperature and humidity — while the temperature of the preceding austral spring is identified as a strong, non-linear carry-over determinant of next-season risk, with colder previous springs associated with substantially higher subsequent risk through mechanisms that remain to be resolved. Proximity to waste-disposal sites contributes additional, partly modifiable risk, and the inverse department-level association with the health-vulnerability index most plausibly reflects the urban–rural transmission and surveillance gradient. For public health practice, the key message is that spatial risk patterns are sufficiently stable and

predictable to guide resource allocation, and that the predictability of both ENSO and the antecedent-spring window opens a realistic path toward early warning with several months of lead time. Prevention planning should concentrate on the identified high-risk departments while establishing enhanced surveillance at the expanding transmission frontier. Future work should integrate continuous ENSO indices and vaccination roll-out, address the overconfidence of the posterior predictive intervals, and pursue finer-resolution analyses capable of resolving intra-urban heterogeneity and distinguishing epidemic from endemic transmission regimes.

List of abbreviations

AR1: first-order autoregressive; AUC: area under the receiver operating characteristic curve; BYM2: Besag–York–Mollié 2; CI: credible interval; ENSO: El Niño–Southern Oscillation; ERA5: fifth-generation ECMWF atmospheric reanalysis; ESA CCI: European Space Agency Climate Change Initiative; ICAR: intrinsic conditional autoregressive; IID: independent and identically distributed; INDEC: Instituto Nacional de Estadística y Censos; INLA: integrated nested Laplace approximation; NB: negative binomial; NBI: Unsatisfied Basic Needs index (Necesidades Básicas Insatisfechas); ONI: Oceanic Niño Index; PAHO: Pan American Health Organization; PC: penalized complexity; PPV: positive predictive value; RH: relative humidity; RR: risk ratio; RW1: first-order random walk; RW2: second-order random walk; SD: standard deviation; SNVS: National Health Surveillance System (Sistema Nacional de Vigilancia de la Salud); VIF: variance inflation factor; WAIC: Watanabe–Akaike information criterion; WHO: World Health Organization; ZINB: zero-inflated negative binomial; ZIP: zero-inflated Poisson.

Declarations

Ethics approval and consent to participate

Not applicable. This study analysed aggregated, de-identified dengue case counts at the administrative department level obtained from the Argentine national health surveillance system, together with publicly

available climatic, environmental and census data; no individual-level data, human participants or human tissue were involved, and no ethics approval was required.

Consent for publication

Not applicable.

Availability of data and materials

The dengue surveillance data analysed for 2018–2025 are openly available through the Argentine national open-data portal (https://datos.gob.ar). The records for 2009–2017 were compiled and provided by the National Directorate of Epidemiology, Ministry of Health of Argentina, and are available from the corresponding author on reasonable request and with the permission of the data providers. ERA5 climate reanalysis data are available from the Copernicus Climate Data Store (https://cds.climate.copernicus.eu); WorldPop gridded population estimates from https://www.worldpop.org; ESA CCI land-cover data from https://www.esa-landcover-cci.org; and INDEC census data from https://www.indec.gob.ar. The analysis code is available from the corresponding author on reasonable request.

Competing interests

The authors declare that they have no competing interests.

Funding

V. Andreo was supported by the Agencia Nacional de Promoción Científica y Tecnológica, Argentina (grant N° 00372–2021). The funder had no role in the study design, data collection and analysis, decision to publish, or preparation of the manuscript.

Authors' contributions

JP conceived and designed the study, performed the statistical analyses, and drafted the manuscript. CL and CM contributed to the study design, methodology, and interpretation of the results. VA contributed to data

acquisition and interpretation. All authors critically revised the manuscript and read and approved the final version.

Acknowledgements

We thank M. Mauriño (Dirección de Epidemiología, Ministerio de Salud de la Nación, Argentina; current address: Institute for Global Health [ISGlobal], Barcelona, Spain) and F. Chesini (Coordinación de Salud Ambiental, Ministerio de Salud de la Nación, Argentina; current address: CONICET-UNDAV, Argentina) for compiling and providing the case data by department.

References

1. World Health Organization. Dengue and severe dengue. Geneva: World Health Organization; 2025. https://www.who.int/health-topics/dengue-and-severe-dengue. Accessed 26 Jun 2026.

2. Messina JP, Brady OJ, Golding N, et al. The current and future global distribution and population at risk of dengue. Nat Microbiol. 2019;4(9):1508-15.

3. Ryan SJ, Carlson CJ, Mordecai EA, Johnson LR. Global expansion and redistribution of Aedes-borne virus transmission risk with climate change. PLoS Negl Trop Dis. 2019;13(3):e0007213.

4. World Health Organization. Dengue – global situation. Disease outbreak news, 30 May 2024. Geneva: World Health Organization; 2024.

5. Pan American Health Organization. Epidemiological update: dengue. Washington, DC: PAHO/WHO; 2024.

6. San Martín JL, Brathwaite O, Zambrano B, et al. The epidemiology of dengue in the Americas over the last three decades: a worrisome reality. Mem Inst Oswaldo Cruz. 2010;105(1):7-16.

7. Grech M, Visintin A, Laurito M, et al. New records of mosquito species (Diptera: Culicidae) from Neuquén and La Rioja provinces, Argentina. Rev Saude Publica. 2012;46(2):387-9.

8. Vezzani D, Carbajo AE. Aedes aegypti, Aedes albopictus, and dengue in Argentina: current knowledge and future directions. Mem Inst Oswaldo Cruz. 2008;103(1):66-74.

9. Rubio A, Cardo MV, Vezzani D, Carbajo AE. Aedes aegypti spreading in South America: new coldest and southernmost records. Mem Inst Oswaldo Cruz. 2020;115:e190496.

10. Obholz G, Mansilla AP, San Blas G, Diaz A. Modeling and updating the occurrence of Aedes aegypti in its southern limit of distribution in South America. Acta Trop. 2024;249:107052.

11. Martín ME, Stein M, Sangermano F, Estallo EL. Ecological niche and potential geographic distribution of Aedes aegypti and Aedes albopictus in Northeast Argentina. Ecohealth. 2025;22:373-86.

12. Rapaport S, Mauriño M, Morales MA, et al. Epidemiology of dengue in Argentina during the 2010/11 to 2019/20 seasons. Trop Med Infect Dis. 2024;9(2):45.

13. Estallo EL, Sippy R, Stewart-Ibarra AM, Grech MG, Benitez EM, Ludueña-Almeida FF, et al. A decade of arbovirus emergence in the temperate southern cone of South America: dengue, Aedes aegypti and climate dynamics in Córdoba, Argentina. Heliyon. 2020;6(9):e04858.

14. Estallo EL, López MS, Ludueña-Almeida FF, Madelón M, Layún F, Robert MA. Increased risks of mosquito-borne disease emergence in temperate regions of South America. Lancet Reg Health Am. 2024;40:100946.

15. Gurevitz JM, Antman JG, Laneri K, Morales JM. Temperature, traveling, slums, and housing drive dengue transmission in a non-endemic metropolis. PLoS Negl Trop Dis. 2021;15(6):e0009465.

16. López MS, Lovino MA, Gómez AA, Rodríguez ST, Radosevich AL, Müller GV, et al. Climate extremes, average conditions and temperature variability as drivers of dengue epidemics in a temperate city of Argentina. J Clim Change Health. 2025;22:100426.

17. Liu-Helmersson J, Stenlund H, Wilder-Smith A, Rocklöv J. Vectorial capacity of Aedes aegypti: effects of temperature and implications for global dengue epidemic potential. PLoS One. 2014;9(3):e89783.

18. Mordecai EA, Caldwell JM, Grossman MK, et al. Thermal biology of mosquito-borne disease. Ecol Lett. 2019;22(10):1690-708.

19. Mordecai EA, Cohen JM, Evans MV, et al. Detecting the impact of temperature on transmission of Zika, dengue, and chikungunya using mechanistic models. PLoS Negl Trop Dis. 2017;11(4):e0005568.

20. Tesla B, Demakovsky LR, Mordecai EA, et al. Temperature drives Zika virus transmission: evidence from empirical and mathematical models. Proc Biol Sci. 2018;285(1884):20180795.

21. Vincenti-Gonzalez MF, Tami A, Lizarazo EF, Grillet ME. ENSO-driven climate variability promotes periodic major outbreaks of dengue in Venezuela. Sci Rep. 2018;8(1):5727.

22. Stewart Ibarra AM, Ryan SJ, Beltrán E, et al. Dengue vector dynamics (Aedes aegypti) influenced by climate and social factors in Ecuador: implications for targeted control. PLoS One. 2013;8(11):e78263.

23. Lowe R, Gasparrini A, Van Meerbeeck CJ, et al. Nonlinear and delayed impacts of climate on dengue risk in Barbados: a modelling study. PLoS Med. 2018;15(7):e1002613.

24. Anyamba A, Chretien JP, Britch SC, et al. Global disease outbreaks associated with the 2015–2016 El Niño event. Sci Rep. 2019;9(1):1930.

25. Cai W, McPhaden MJ, Grimm AM, et al. Climate impacts of the El Niño–Southern Oscillation on South America. Nat Rev Earth Environ. 2020;1(4):215-31.

26. González MH, Skansi MM, Garbarini EM, Rolla AL. ENSO influence over precipitation in Argentina. In: Daniels JA, editor. Advances in environmental research, vol. 52. New York: Nova Science Publishers; 2016. p. 223-46.

27. Grimm AM, Barros VR, Doyle ME. Climate variability in southern South America associated with El Niño and La Niña events. J Clim. 2000;13(1):35-58.

28. Powell JR, Tabachnick WJ. History of domestication and spread of Aedes aegypti — a review. Mem Inst Oswaldo Cruz. 2013;108(Suppl 1):11-7.

29. Getachew D, Tekie H, Gebre-Michael T, et al. Breeding sites of Aedes aegypti: potential dengue vectors in Dire Dawa, East Ethiopia. Interdiscip Perspect Infect Dis. 2015;2015:706276.

30. Padmanabha H, Soto E, Mosquera M, et al. Ecological links between water storage behaviors and Aedes aegypti production: implications for dengue vector control in variable climates. Ecohealth. 2010;7(1):78-90.

31. Barrera R, Avila J, González-Téllez S. Unreliable supply of potable water and elevated Aedes aegypti larval indices: a causal relationship? J Am Mosq Control Assoc. 1995;11(2):189-94.

32. Shepard DS, Undurraga EA, Halasa YA, Stanaway JD. The global economic burden of dengue: a systematic analysis. Lancet Infect Dis. 2016;16(8):935-41.

33. Undurraga EA, Betancourt-Cravioto M, Ramos-Castañeda J, et al. Economic and disease burden of dengue in Mexico. PLoS Negl Trop Dis. 2015;9(3):e0003547.

34. Ministerio de Salud de la Nación. Vigilancia epidemiológica de dengue — datos abiertos [dataset]. Buenos Aires: Ministerio de Salud de la Nación; 2025. https://datos.gob.ar. Accessed 26 Jun 2026.

35. Tatem AJ. WorldPop, open data for spatial demography. Sci Data. 2017;4:170004.

36. WorldPop. Global high resolution population denominators project (~1 km gridded population estimates). Southampton: School of Geography and Environmental Science, University of Southampton; 2018. https://www.worldpop.org.

37. Hersbach H, Bell B, Berrisford P, et al. The ERA5 global reanalysis. Q J R Meteorol Soc. 2020;146(730):1999-2049.

38. Lawrence MG. The relationship between relative humidity and the dewpoint temperature in moist air: a simple conversion and applications. Bull Am Meteorol Soc. 2005;86(2):225-33.

39. Trenberth KE. The definition of El Niño. Bull Am Meteorol Soc. 1997;78(12):2771-8.

40. ESA. Land cover CCI product user guide version 2. 2017. https://www.esa-landcover-cci.org. Accessed 26 Jun 2026.

41. Moore TC, Brown HE. Estimating Aedes aegypti (Diptera: Culicidae) flight distance: meta-data analysis. J Med Entomol. 2022;59(4):1164-70.

42. Instituto Nacional de Estadística y Censos (INDEC). Censo Nacional de Población, Hogares y Viviendas. Buenos Aires: INDEC; 2010 and 2022.

43. Rue H, Martino S, Chopin N. Approximate Bayesian inference for latent Gaussian models by using integrated nested Laplace approximations. J R Stat Soc Series B Stat Methodol. 2009;71(2):319-92.

44. Blangiardo M, Cameletti M. Spatial and spatio-temporal Bayesian models with R-INLA. Chichester: John Wiley & Sons; 2015.

45. Riebler A, Sørbye SH, Simpson D, Rue H. An intuitive Bayesian spatial model for disease mapping that accounts for scaling. Stat Methods Med Res. 2016;25(4):1145-65.

46. Simpson D, Rue H, Riebler A, Martins TG, Sørbye SH. Penalising model component complexity: a principled, practical approach to constructing priors. Stat Sci. 2017;32(1):1-28.

774 47. Dormann CF, Elith J, Bacher S, Buchmann C, Carl G, Carré G, et al. Collinearity: a review of methods to deal
775 with it and a simulation study evaluating their performance. Ecography. 2013;36(1):27-46.
776 48. Lowe R, Lee SA, O'Reilly KM, et al. Combined effects of hydrometeorological hazards and urbanisation on
777 dengue risk in Brazil: a spatiotemporal modelling study. Lancet Planet Health. 2021;5(4):e209-19.
778 49. Cheng Q, Jing Q, Spear RC, et al. The interplay of climate, intervention and imported cases as determinants of the
779 2014 dengue outbreak in Guangzhou. PLoS Negl Trop Dis. 2020;14(2):e0008056.
780 50. Caprara A, Lima JWdeO, Marinho ACP, Nobre CM, Sommerfeld J, Kroeger A. Irregular water supply, household
781 usage and dengue: a bio-social study in the Brazilian Northeast. Cad Saude Publica. 2009;25(Suppl 1):S125-36.
782 51. Fischer S, De Majo MS, Di Battista C, Campos RE. Effects of temperature and humidity on the survival and
783 hatching response of diapausing and non-diapausing Aedes aegypti eggs. J Insect Physiol. 2025;161:104726.
784 52. Mensch J, Di Battista C, De Majo MS, Campos RE, Fischer S. Increased size and energy reserves in diapausing
785 eggs of temperate Aedes aegypti populations. J Insect Physiol. 2021;131:104232.
786 53. Diniz DFA, de Albuquerque CMR, Oliva LO, de Melo-Santos MAV, Ayres CFJ. Diapause and quiescence:
787 dormancy mechanisms that contribute to the geographical expansion of mosquitoes and their evolutionary
788 success. Parasit Vectors. 2017;10:310.
789 54. Morlighem C, Visée C, Nnanatu CC, Tine MW, Diène AN, Linard C. Leveraging routine health facility data for
790 space-time modelling of malaria incidence at the catchment level in Senegal. Preprints. 2025.
791 https://doi.org/10.20944/preprints202506.0590.v1.
792 55. Chen Y, Li N, Lourenço J, Wang L, Cazelles B, Dong L, et al. Measuring the effects of COVID-19-related
793 disruption on dengue transmission in southeast Asia and Latin America: a statistical modelling study. Lancet
794 Infect Dis. 2022;22(5):657-67.
795 56. Held L, Schrödle B, Rue H. Posterior and cross-validatory predictive checks: a comparison of MCMC and INLA.
796 In: Kneib T, Tutz G, editors. Statistical modelling and regression structures — Festschrift in honour of Ludwig
797 Fahrmeir. Heidelberg: Physica-Verlag; 2010. p. 91-110.
798 57. Andreo V, Porcasi X, Guzman C, Lopez L, Scavuzzo CM. Spatial distribution of Aedes aegypti oviposition
799 temporal patterns and their relationship with environment and dengue incidence. Insects. 2021;12(10):919.

58. Espinosa M, Weinberg D, Rotela CH, Polop F, Abril M, Scavuzzo CM. Temporal dynamics and spatial patterns of Aedes aegypti breeding sites, in the context of a dengue control program in Tartagal (Salta Province, Argentina). PLoS Negl Trop Dis. 2016;10(5):e0004621.